Earth and Planetary Science Letters 304 (2011) 29–35

Contents lists available at ScienceDirect

Earth and Planetary Science Letters

journal homepage: www.elsevier.com/locate/epsl

Relationship of compaction bands in Utah to Laramide fault-related folding

Richard A. Schultz

Geomechanics—Rock Fracture Group, Department of Geological Sciences and Engineering/172, University of Nevada, Reno NV 89557, United States

ARTICLE INFO

Article history:
Received 8 July 2010
Received in revised form 28 November 2010
Accepted 6 January 2011
Available online 21 February 2011

Editor: L. Stixrude

Keywords:
compaction band
deformation band
East Kaibab monocline
thrust tectonics

ABSTRACT

Multiple sets of compaction bands of southwestern Utah occur in Navajo Sandstone near a bend in the adjacent East Kaibab monocline. Forward mechanical models of blind-thrust fault deformation are used in this paper to investigate the spatial relationship between compaction bands and fault-related folding. Results are consistent with the East Kaibab monocline being underlain by a west-dipping blind high-angle reverse fault between ~1.5 and 5 km depth below the top of the Navajo Sandstone. Reverse slip along this reactivated fault during the Laramide orogeny is inferred to have produced values of compactional normal strain that were largest in the footwall near the concave map-view bend in the monocline. The calculated compactional normal strains and Coulomb stress increases are consistent with the field occurrence of pure and shear-enhanced compaction bands in this area. Bends, relays, stepovers, or other geometric complexities above blind reverse faults are thus inferred to be potential sites for compaction band localization in appropriate rock types.

1. Introduction

Compaction bands are a type of deformation band characterized by predominantly compactional (closing) strains that form in high-porosity sandstone (e.g., Aydin et al., 2006; Mollema and Antonellini, 1996; Schultz and Fossen, 2008; Tembe et al., 2008). These thin structures define a geologically interesting and understudied class of strain localization in rock that can impede subsurface fluid flow and thus are also important to groundwater and petroleum extractions (e.g., Holcomb et al., 2007). Several distinct types and sets of compaction bands are known from the Buckskin Gulch site in southwestern Utah (Mollema and Antonellini, 1996; Schultz, 2009; Schultz et al., 2010) and the Valley of Fire State Park site in southern Nevada (Eichhubl et al., 2010; Sternlof et al., 2005), including wiggly, pure compaction bands and thick, planar, shear-enhanced compaction bands. Compaction bands are currently under active study worldwide using theoretical, experimental, and field techniques. Discussions of compaction localization in porous rocks are given by Baud et al. (2006), Bésuelle (2001), Bésuelle and Rudnicki (2004), Eichhubl et al. (2010), and Holcomb et al. (2007).

The Buckskin Gulch site in Utah occurs adjacent to the East Kaibab monocline (Fig. 1), one of several large anticlines within the Colorado Plateau of the western United States (see Davis and Bump, 2009 for a recent overview). The East Kaibab monocline is thought to be underlain by a blind high-angle fault, originally having normal offset, that was reactivated with reverse offset during the Laramide orogeny (e.g., Doelling and Willis, 2006; Huntoon, 1993), leading to the growth of the East Kaibab monocline and the localization of various structures, such as the deformation band arrays, above the blind fault tip (e.g., Tindall, 2000; Tindall and Davis, 1999). Although compaction bands were not discussed in those studies, the bands occur in areas adjacent to the East Kaibab monocline where a causal relationship between thrusting along the subjacent blind fault and shear deformation bands to its east has been suggested (e.g., Davis, 1999). The compaction bands are located where the East Kaibab monocline abruptly changes trend, from north–northeast to more northeasterly (Fig. 1) and occur not only in nearly flat-lying strata to the east of the monocline (Fig. 2) but up on its forelimb as well (Mollema and Antonellini, 1996; Schultz, unpublished data).

Theoretical and experimental works indicate that compaction-related deformation of porous granular rocks can be initiated for particular combinations of stress state (i.e., axisymmetric loading), loading paths, mean stress, and evolving material properties (e.g., Bésuelle and Rudnicki, 2004; Issen and Challa, 2008). Although the prediction of compaction band nucleation in continuum mechanics theory and experiments has continued to prove challenging, it is also difficult to apply these results to field situations where stress states, loading paths, and rock properties during the deformation are less well known (e.g., Aydin and Ahmadov, 2009; Eichhubl et al., 2010; Holcomb et al., 2007). Similarly, the major characteristics of subsurface faults beneath the East Kaibab monocline are largely unknown. For example, Doelling and Davis (1989) place an east-dipping normal fault beneath the anticline, whereas Huntoon (1993), Tindall and Davis (1999), and Tindall (2000) infer a west-dipping normal fault reactivated as a high-angle reverse fault (see also Doelling and Willis, 2006). In neither case is the depth of faulting known independently from geophysical or other data, nor is information on

E-mail address: schultz@mines.unr.edu.

0012-821X/$ – see front matter © 2011 Elsevier B.V. All rights reserved.
doi:10.1016/j.epsl.2011.01.001

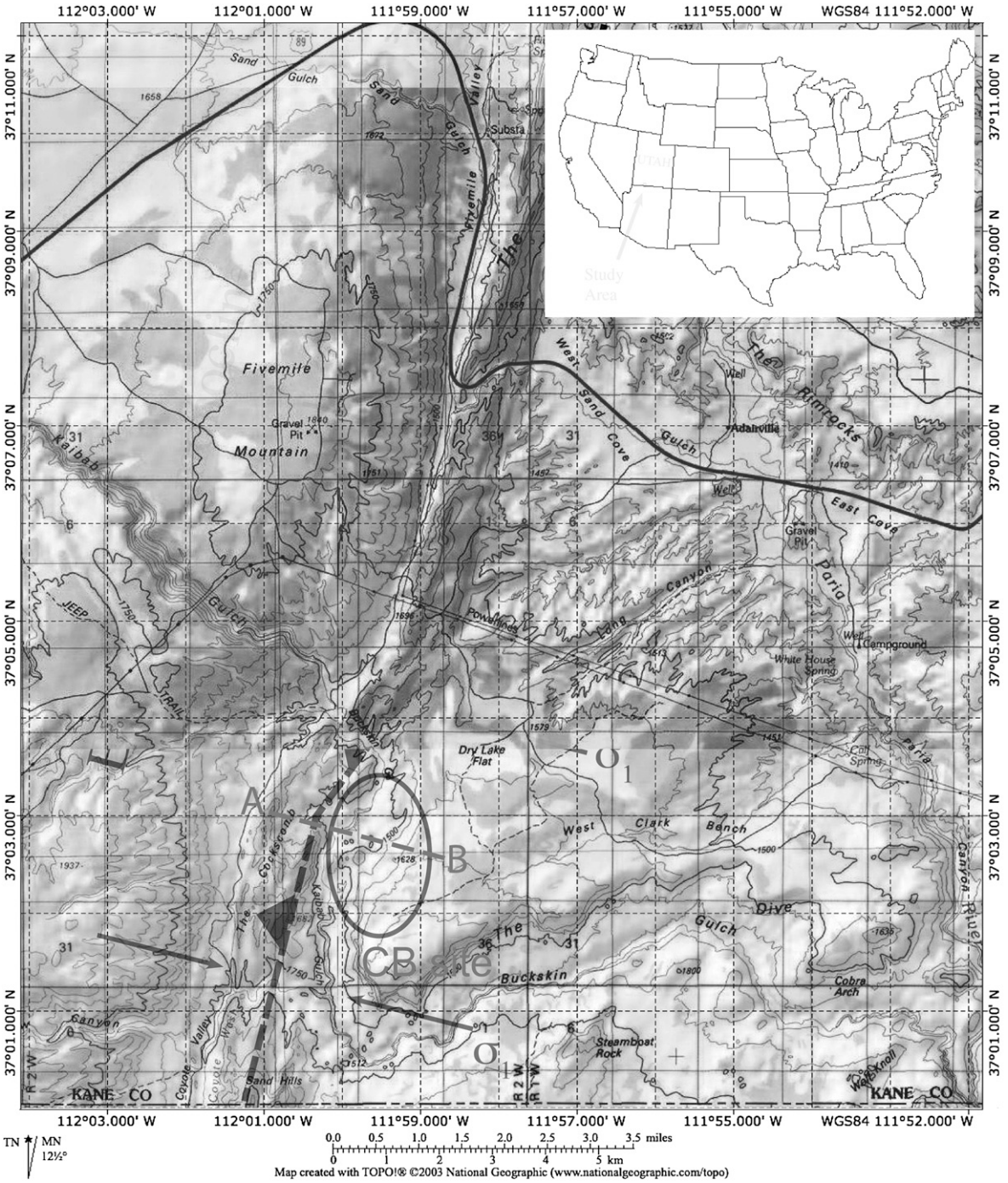

Fig. 1. Location of the Utah compaction band site (circled) in relation to the East Kaibab monocline. Possible locations of nearby blind reverse faults near the Cockscomb and field areas are shown (filled triangles on hanging walls; blind faults are dashed). Location of cross-sectional slice for the three-fault calculation suite shown by dashed line. A–B. Topographic map base generated using Topo! software and 1983 North America datum; magnetic declination 12.5°.

fault segmentation or slip distribution available. However, the pattern of the East Kaibab monocline near the Utah site is consistent with a pair of north–northeast striking, west-dipping, blind thrust or reverse faults separated by a linked relay or stepover beneath the northeasterly trending segment, following Shamir and Eyal's (1995) and Roznovsky and Aydin's (2001) works on segmented monoclines in Israel and Utah.

In contrast, a correspondence exists between laboratory experiments and grain-scale mechanics on compaction band propagation and localized compactional strains (e.g., Katsman and Aharonov, 2006; Katsman et al., 2004; Stanchits et al., 2009; Vajdova and Wong, 2003). Utilizing this set of results, a simple mechanical model of fault-related folding is adopted in this paper to investigate possible subsurface fault geometries beneath the East Kaibab monocline. The spatial relationship between compaction bands and the East Kaibab monocline is then examined to assess whether the bands may correspond to areas of calculated compactional strain from the models. The analysis assumes constant elastic rock properties and related parameters, which have been shown in other studies to be suggestive of the characteristics of initial rock yielding or failure in natural systems having higher values of final strain (e.g., King et al., 1994; Okubo and Schultz, 2004, 2005). The results suggest that reverse displacement along a blind high-angle fault can promote the development of compaction-related deformation adjacent to a surficial monocline.

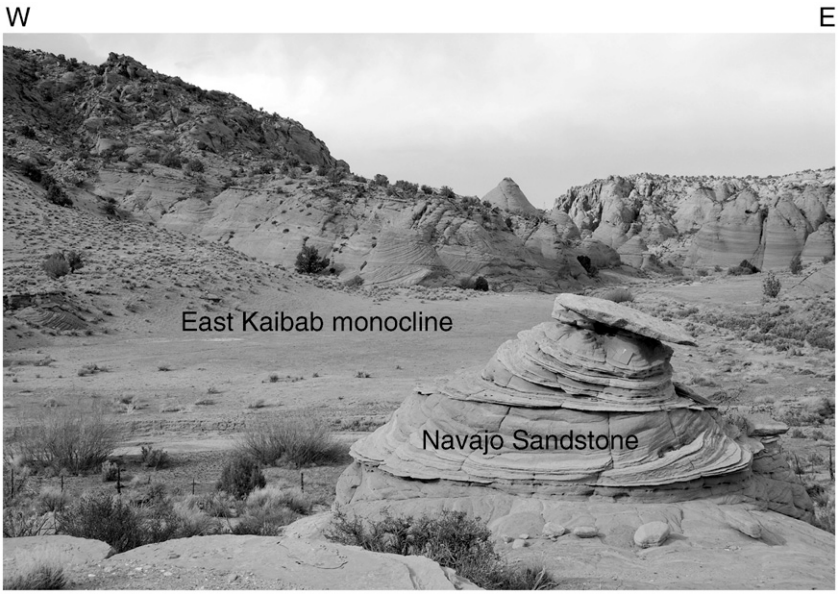

Fig. 2. Photograph of part of the East Kaibab monocline, looking toward the north, showing beds decreasing in dip to become sub-horizontal to the east. Compaction bands occur in the Navajo Sandstone across the entire frame and for another ~1 km to the east. Frame width ~1.5 km.

2. Location and previous work

The Buckskin Gulch site in southwestern Utah (Mollema and Antonellini, 1996; Schultz, 2009) exposes a rich assemblage of compaction bands and related deformation band shear zones in the uppermost part of the Jurassic Navajo Sandstone (Fig. 1). The depth of burial at the time of compaction band formation (Schultz et al., 2010) was approximately 0.9–1.7 km from stratigraphic and band-thickness relationships (Schultz, 2009; Solum et al., 2010). The cross-bedded sandstone sequences that host compaction bands are characterized by large average grain size, well sorted grains, and high porosity (Mollema and Antonellini, 1996; Schultz, 2009; Schultz et al., 2010) associated with a nonmarine depositional environment (i.e., eolian migrating dunes).

Deformation of the Navajo Sandstone resulted in several sets of structures at the Utah site including: (1) deformation band shear zones (DBSZs) having thrust or reverse senses of offset (Schultz, unpublished data), and (2) pure and shear-enhanced compaction bands. Small shearing offsets having reverse sense were observed along thick compaction bands at the Utah site by Mollema and Antonellini (1996) and Schultz et al. (2010), motivating the interpretation of these structures as shear-enhanced compaction bands oriented at some non-zero angle to the far-field maximum horizontal compressive principal stress (see Eichhubl et al., 2010 for analogous structures and interpretations from the Nevada site). Field relations demonstrate that the wiggly pure compaction bands generally form within the same deformation sequence as the thicker shear-enhanced compaction bands (Schultz et al., 2010).

Petrographic analyses demonstrate porosity reduction normal to the plane of a compaction band (e.g., Eichhubl et al., 2010; Mollema and Antonellini, 1996; Sternlof et al., 2005). Compactional strain within pure and shear-enhanced compaction bands is accommodated at both the Utah and Nevada sites primarily by grain reorganization with minor fragmentation and plastic grain deformation (Eichhubl et al., 2010; Mollema and Antonellini, 1996; Schultz et al., 2010; Sternlof et al., 2005).

Compaction bands at the Utah site strike ~N15°E (Schultz, 2009) and dip subvertically (for pure compaction bands) or ~50–60° (for shear-enhanced compaction bands) (Schultz et al., 2010). The maximum remote compressive stress σ_1 associated with compaction band formation thus was subhorizontal with an azimuth of ~285°. The azimuth of σ_1 is approximately perpendicular to the local strike of the East Kaibab monocline just to the west of the site (Fig. 1). This angular relationship implies that more northerly trending blind fault segments inferred beneath the monocline near the Buckskin Gulch site accommodated primarily reverse offsets, with little or no oblique (strike-slip) component along those segments at the time of compaction band deformation. The inferred compression direction of 285° is also remarkably similar to the relative paleomotion direction of the subducting Farallon plate in this area (Humphreys, 2009), implying a correspondence between stresses due to shallow slab subduction at depth and those inducing reverse-fault offsets beneath the East Kaibab monocline (see parallel conclusions for the Waterpocket fold by Roznovsky and Aydin, 2001), and compaction band deformation, nearer the surface.

3. Approach

A causal relationship between growth of the East Kaibab monocline and the occurrence of compaction bands was investigated in this paper by using the numerical modeling software package Coulomb (http://quake.usgs.gov/research/deformation/modeling/coulomb/overview.html). This three-dimensional forward mechanical dislocation model calculates the stresses and displacements in an elastic half-space due to displacements that are specified along faults in the subsurface (see Toda et al., 1998, 2007; also Fossen et al., 2010, Schultz, 2000; Schultz, 2003, Schultz and Lin, 2001; and Schultz and Watters, 2001 for details on the approach and applications to normal fault and thrust fault systems). The approach is comparable to the dislocation solution used by Shamir and Eyal (1995) who evaluated monocline and fold patterns in relation to subsurface faulting. Using a mechanical model for fault-related folding and related deformation, as done in this paper, provides insight into the development of structural topography and deformation beyond that obtained from analog or kinematic trishear models of fault-related deformation (e.g., Johnson and Johnson, 2002).

A suite of calculations was performed to explore the influence of fault geometries in the subsurface to the prediction of compaction bands near a monocline. The first suite examined the role of fault dips of 30°, corresponding to blind thrust faults, and 60°, corresponding to pre-existing normal faults reactivated during the Late Cretaceous to Paleocene Laramide orogeny (e.g., Humphreys, 2009) as high-angle

reverse faults (e.g., Bump and Davis, 2003; Doelling and Willis, 2006; Huntoon, 1993). A blind thrust or reactivated reverse fault was defined for this suite as 20 km in horizontal length, dipping at 30° or 60° to the west, with its upper tip at 1.5 or 2.0 km below the surface and its lower tip, corresponding to the depth of faulting, at 5 km or 10 km below the surface. A reverse displacement of 100 m is applied along the fault, with linear tapering of the displacement distribution both horizontally and vertically in order to remove large stress or strain changes near the fault edges (see Toda et al., 2007, for details of the procedure). Larger values of reverse displacement would increase fold amplitudes but otherwise not change the results significantly. The host rock is represented by a Young's modulus of 20 GPa, Poisson's ratio of 0.25, and friction coefficient of 0.6, values that are consistent with those of sedimentary rocks such as the Navajo Sandstone (e.g., Schultz, 2009; Sternlof et al., 2005). A horizontal observation grid in the *xy*-plane measuring 60×30 km is placed at a depth of 1 km, simulating deformation in the upper part of the Navajo Sandstone, with calculations performed at a regular spacing of 100 m. Although the specific values of fault dimensions, offsets, dip angles, grid depth, and host rock properties affect the results presented below in detail, exploration of the parameter space shows that the conclusions of the analysis are not changed substantially by reasonable variations in these values. As a result, the conclusions should apply to the East Kaibab monocline as well as to other blind-thrust anticlines.

Based on the results of the initial suite, a second suite of calculations was run that incorporated a more complex fault geometry at depth beneath the monocline. In this suite three blind faults were specified, with two echelon faults linked across the relay by a third fault oriented at 30° to the strike of the echelon faults, based on the map-view geometry of the East Kaibab monocline (see inferred fault pattern in Fig. 1). As in the previous suite, dip angles of 30° and 60° to the west were investigated, with the upper and lower fault tips set at 1.5 km and 5 km, respectively. A net reverse displacement of 100 m was again defined on the two echelon faults with the oblique slip partitioned on the linking fault into 87 m of reverse offset and 50 m of right-lateral strike-slip offset as defined by trigonometry.

The lower fault tip is represented in this analysis as a rapid reduction in fault displacement to zero at the depth of faulting (e.g., Shamir and Eyal, 1995). For a thrust fault that may sole into a shallow décollement at this depth, a bend in the fault geometry is well represented by using this approach (e.g., Okubo and Schultz, 2004). For a normal fault reactivated as a high-angle reverse fault, the lower tip may either be the physical fault tip or a reduction of dip angle into a shallow detachment surface at this depth. In either case, the calculations presented for the observation plane located at a shallow depth in this paper are most sensitive to the depth to the upper fault tip and the magnitude of the fault displacement, and do not depend on potential translation along a sub-horizontal décollement or detachment surface.

Three physical quantities were calculated to assess the contribution of a fault-cored anticline to compaction band formation. First, vertical displacements of the observation grid were calculated, corresponding to the structural topography of a deformed horizon. This quantity provides an indication of the size and geometry of the anticline generated above the blind fault (e.g., Okubo and Schultz, 2004; Savage and Cooke, 2004; Schultz, 2000; Schultz and Watters, 2001; Shamir and Eyal, 1995). Second, the dilational strain (Paterson and Wong, 2005; variously called dilation, as in this paper, or dilatation in seismotectonics and in the Coulomb program: Toda et al., 2007) is calculated from the elastic normal strain components in each of the three coordinate directions (dilation $= \varepsilon = \varepsilon_{xx} + \varepsilon_{yy} + \varepsilon_{zz}$). Because compaction bands accommodate contractional strains across them, this quantity was investigated as a proxy for predicting their occurrence in areas near a fault-cored anticline (i.e., $\varepsilon<0$ for compaction, Paterson and Wong, 2005). The background value of ε, in the absence of deformation, can be estimated by setting $\sigma_x = \sigma_y = \sigma_z = \sigma_v$ in the equations for ε to obtain $\varepsilon_0 = 3\rho g z(1-2\nu)/E$, in which ρ is the effective density of the overlying stratigraphic section, g is gravitational acceleration, z is depth, ν is Poisson's ratio, and E is Young's modulus. Using values of $\rho = (2250–1000 = 1250\ \mathrm{kg/m^3})$, $g = 9.8\ \mathrm{m/s^2}$, $\nu = 0.2$, and $E = 20$ GPa, $\varepsilon_0 = 1.1\times10^{-3}$ at 1 km depth. The third quantity, change in Coulomb failure stress, quantifies the tendency for frictional sliding along potential shear planes (e.g., King and Cocco, 2001; King et al., 1994; Lin et al., 2010; Schultz, 2000; Stein, 1999; Stein et al., 1992). This quantity can also be interpreted as the tendency for pre-peak inelastic yielding in shear, rather than frictional sliding, within a porous sandstone (e.g., Davis and Selvadurai, 2002, p. 95; Paterson and Wong, 2005, p. 252). By specifying optimum thrust fault plane orientations, this quantity reveals areas near a fault-cored anticline where thrust-related shearing may be favored in the deforming strata.

4. Results and Discussion

The topography of the anticline formed above the upper tip of a blind reverse fault depends on the dip angle of the underlying fault, as shown in Fig. 3 (e.g., Okubo and Schultz, 2004; Schultz and Watters, 2001; Shamir and Eyal, 1995; Taboada et al., 1993). The width of the anticline above a shallow dipping (30°) thrust fault (Fig. 3a) is larger than for a steep dipping reactivated fault ($\delta = 60°$, also having a comparable magnitude of reverse offset; Fig. 3b). Given the relatively narrow cross-strike width of the East Kaibab monocline, it is plausible that the underlying fault dips more steeply than 30°, and perhaps as great as 60°, although the precise width of the monoclinal fold is uncertain given its uneven present-day exposure. East-dipping faults (e.g., Doelling and Davis, 1989) produce topographies that are not consistent with that observed across the monocline in this area.

Decreasing the depth of the upper blind tip has the effect of increasing the amplitude of structural topography. Increasing the depth of the lower tip increases both the amplitude and the width of the structural topography (Fig. 4a). The width of the anticline is

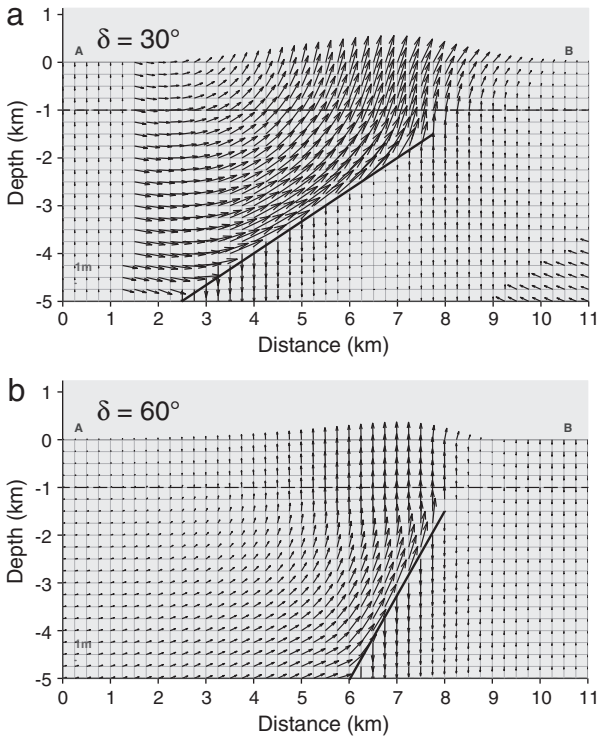

Fig. 3. Calculated displacement vectors in cross-sectional view for a (a) 30° dipping blind thrust fault and (b) 60° dipping blind reactivated reverse fault. The width of the anticline is reduced as the fault dip increases.

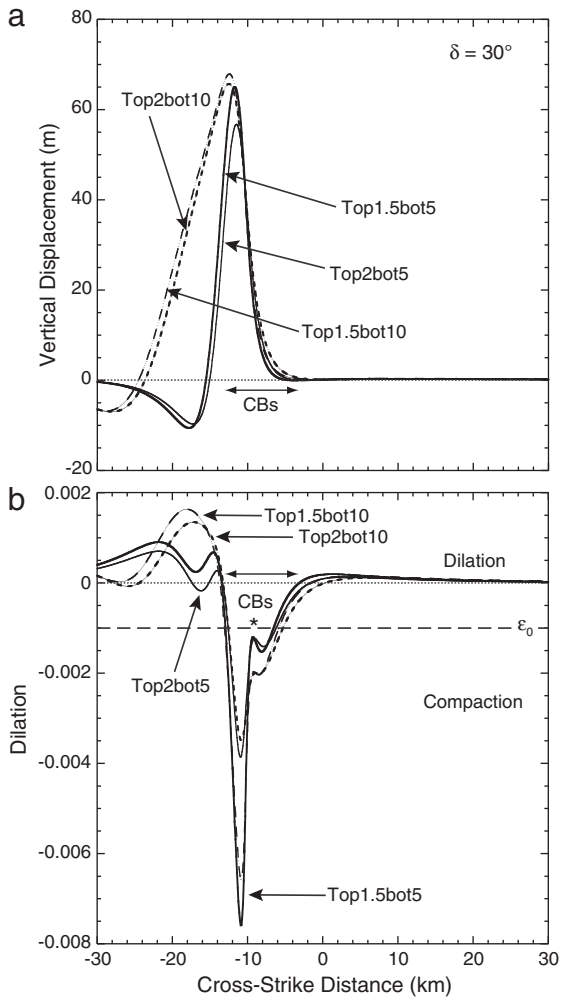

Fig. 4. Cross-sectional slices through the fault's map-view midpoint showing detail of (a) calculated structural topography and (b) dilational strain, for 30° dipping blind thrust fault. Asterisk marks the location of the upper tip of the blind fault at the depth of the observation plane. Compaction bands may be predicted for negative values of dilation (arrows); background value of dilational strain ε_0 shown by dashed line.

reduced by about half as the depth of faulting decreases from 10 km to 5 km, suggesting that the relatively narrow East Kaibab monocline may be more consistent with a smaller depth of faulting, such as 5 km, than with a greater depth, such as 10 km. Decreasing the depth of the upper blind fault tip from 2 km to 1.5 km, corresponding to depths of 1–0.5 km below the observation plane, has little effect on either the structural topography or the dilational strain (Fig. 4) except for increasing the absolute values of both quantities somewhat.

Dilational strain is modestly positive (indicating volumetric increase) except above the blind fault tip (location shown by the * in Fig. 4b). The area vertically above the fault tip is characterized by significant local compaction ($\varepsilon<0$) and volume reduction in the host rocks. Given the correspondence between the predicted locations of strongly negative dilation and the general location of compaction bands at the Utah site, this quantity can be considered to help predict the occurrence of pure, and perhaps shear-enhanced, compaction bands in sufficiently porous, coarse-grained, well-sorted rocks such as the Navajo Sandstone (Fig. 4b, arrow). The location along the blind-thrust anticline where compaction bands may be favored is along its forelimb (Fig. 4a, double-sided arrow labeled CBs).

The predicted structural topography and dilational strain for a reactivated fault ($\delta=60°$) are similar to those presented for the shallow blind thrust fault case. The amplitude and width of the anticline are reduced above the steeply dipping reactivated fault (Figs. 3b and 4b) relative to the shallow thrust fault case. The dilation shows a similar pattern although the peak corresponding to the location of the upper blind fault tip (* in Fig. 4b) has become positive (dilational) rather than negative (compactional; Fig. 5b). As a result, the horizontal, cross-strike extent of compaction bands that would be predicted by using this criterion is considerably reduced, corresponding to only a small horizontal strip along the anticline's forelimb (Fig. 5a, arrow labeled CBs).

Based on the foregoing results, fault geometries with blind upper tips at 1.5 km depth, lower tips at 5 km depth, and dip angles of 30° and 60° were investigated further. The change in calculated Coulomb failure stress for both cases was calculated for a typical value of rock frictional resistance ($\mu=0.6$, Fig. 6). Shearing along optimally oriented planes is predicted to occur just above, and beyond, the location of the upper fault tip, regardless of fault dip angle. By comparing Figs. 4, 5, and 6, this area corresponds primarily to the forelimb of the anticline. The large magnitudes of Coulomb failure stress imply that reverse-sense shearing in the cover rocks would occur early in the deformation, perhaps before the magnitude of reverse displacement on the subjacent fault reached the value of 100 m used in this analysis. Such shearing would contribute to shear-enhanced compaction and deformation band damage zones in the anticline's forelimb.

The second suite of calculations modeled a linked array of three blind faults having upper tips at 1.5 km depth, lower tips at 5 km depth, and

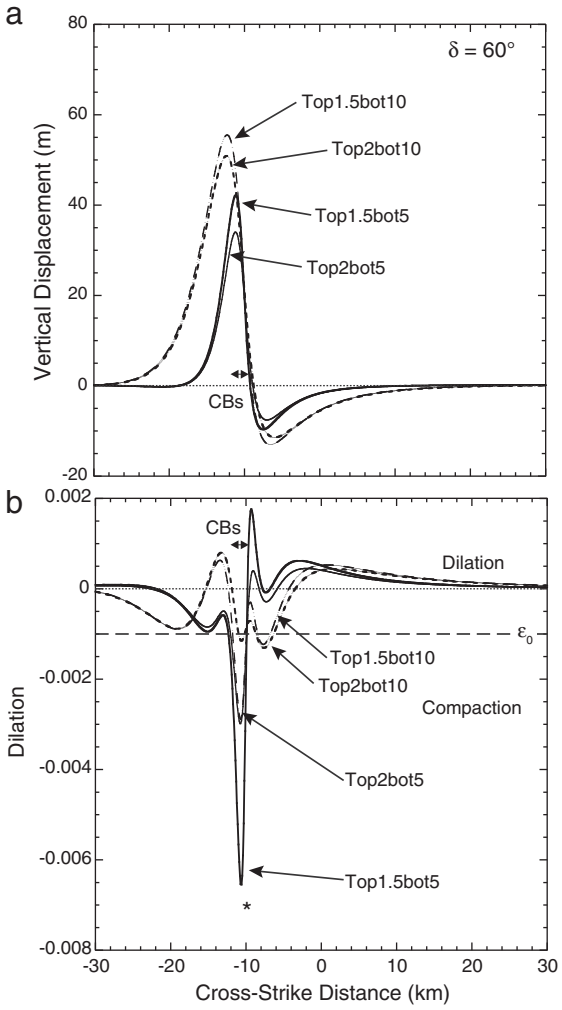

Fig. 5. Cross-sectional slices through the fault's map-view midpoint showing detail of (a) calculated structural topography and (b) dilational strain, for 60° dipping blind reactivated fault. Asterisk as in Fig. 4. Compaction bands may be predicted for negative values of dilation (arrows); background value of dilational strain ε_0 shown by dashed line.

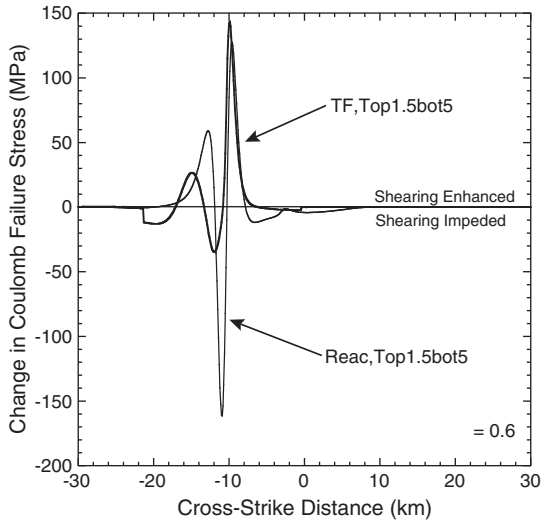

Fig. 6. Change in Coulomb failure stress calculated along cross-sectional slices in Figs. 4 and 5 for 30° dipping blind thrust fault (labeled TF,Top1.5bot5 in the figure) and for 60° dipping blind reactivated reverse fault (labeled Reac,Top1.5bot5 in the figure) for host rock friction coefficient of $\mu = 0.6$.

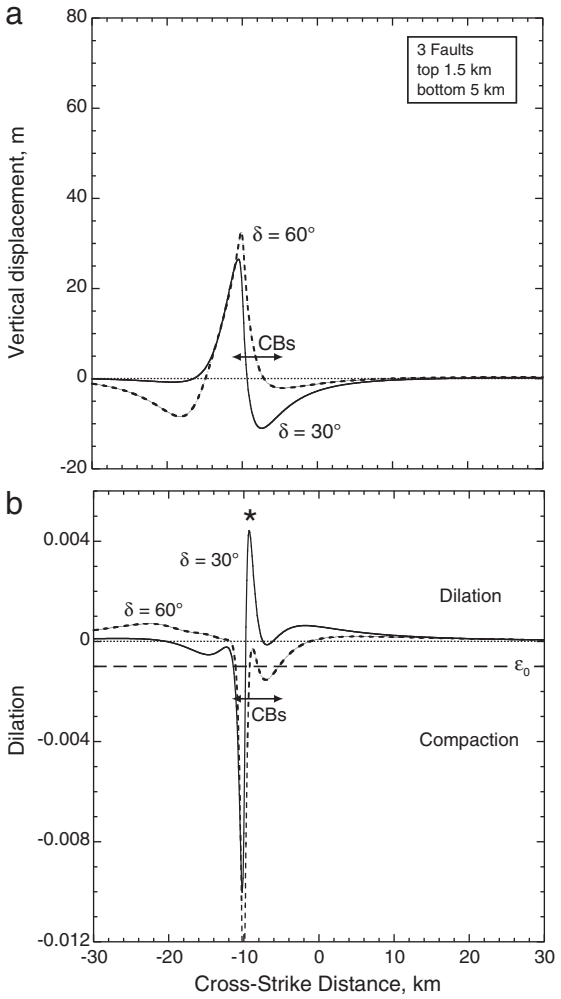

Fig. 7. Cross-sectional slices through the three-fault array (location shown in Fig. 1, cross-sectional slice through circled area) showing detail of (a) calculated structural topography and (b) dilational strain, for 60° dipping blind reactivated reverse faults. Asterisk as in Figs. 4 and 5. Compaction bands may be predicted for negative values of dilation (arrows); background value of dilational strain ε_0 shown by dashed line.

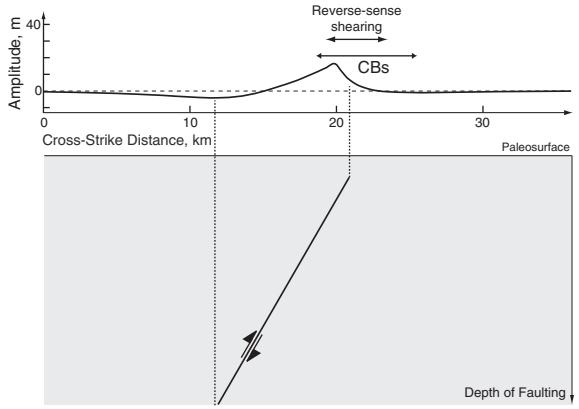

Fig. 8. Schematic cross section illustrating predicted location of the compaction bands and related reverse-sense shearing within the Navajo Sandstone in relation to the location of the upper tip of the subjacent blind fault. Monocline shape (upper panel) redrawn from the reactivated reverse fault case in Fig. 7a. Lower panel shows reactivated fault with positions of upper and lower tips correlated to superjacent anticline; depth axis not to scale. Arrows show predicted locations of reverse-sense shearing and compaction bands (CBs) for 1 km depth from Figs. 6 and 7, respectively.

dip angles of 30° and 60°. The results, shown in Fig. 7, are comparable to those already presented for an individual blind fault, except that compaction bands are predicted unequivocally only for the reactivated fault case (60° fault dip angles). The difference between this result and the previous results, for the single fault cases, lies in the increased value of compactional strain due to slip along the right-oblique blind reverse linking segment (see Fig. 1). As a result, the bend in the East Kaibab monocline, associated with the blind fault geometry shown in Fig. 1, would lead to an enhanced compactional strain in the area corresponding to the Buckskin Gulch site, paralleling the relationship inferred for monoclinal bends and shearing deformation bands by Roznovsky and Aydin (2001). Such bends, jogs, stepovers, or other geometric irregularities along subjacent reverse faults may then be the most favorable sites along an irregular fault-cored anticline or monocline for compaction banding given host rocks with the appropriate petrophysical properties. By contrast, calculations performed for two echelon unlinked blind thrust or reverse faults (not shown) suggest negligible enhancement of compactional strain near the corresponding location of the compaction band site.

Results from the modeling work are summarized in Fig. 8. The geometry of the blind reverse fault, specifically its dip angle, is critical to the prediction of compaction bands in the anticline above. Compaction bands are predicted to be associated with the location of the upper tip of a blind reverse fault, with their lateral, cross-strike extent influenced by several factors including the dip angle of the subjacent fault, the depth of the upper fault tip below the horizon of interest, and the map-view configuration of the fault (i.e., bent or linked faults with oblique displacement components). For a fold such as the East Kaibab monocline, which has an irregular map-view geometry, compaction bands may be suggested to occur (given appropriate host rocks) in narrow bands on the monoclinal forelimb that broaden into wider zones at concave bends in the fold.

5. Conclusions

Mechanical modeling of the East Kaibab monocline suggests that it is underlain by a west-dipping, blind high-angle fault with a reverse sense of offset. The results presented in this paper then provide insight into the occurrence of the compaction bands near the monocline. By calculating the elastic dilational normal strain and Coulomb failure stress in the vicinity of a blind thrust or reverse fault, pure and shear-enhanced compaction bands are inferred to be associated with areas of greatest negative elastic dilational strain (i.e., compaction) and Coulomb stress

increase. The good correspondence between the simple mechanical analysis presented in this paper and the field occurrence of compaction bands at the Utah site suggests that a more complete analysis of compaction band localization near the East Kaibab monocline, that incorporates evolving material properties and stress states, may be warranted.

In addition to a thrust-faulting tectonic environment associated with growth of the East Kaibab monocline above a blind reverse fault, relays, irregularities, and bends along the trace of blind reverse faults or their surficial anticlines appear to be important in the localization of compaction bands. In particular, the eastward change in trend of the East Kaibab monocline, associated with a concave re-entrant with reverse and right-oblique offsets on subjacent linked high-angle blind fault segments, predicts enhanced elastic compactional strain in the footwall area that correlates with the location of the Utah site. By implication, pure or shear-enhanced compaction bands may occur in conjunction with complexities in the traces of linked blind thrust or high-angle reverse faults in their relay or stepover regions as long as the *in situ* stress states and rock properties are also favorable to compaction band localization.

Acknowledgements

Reviews by Peter Eichhubl and an anonymous referee, plus comments by Haakon Fossen, sharpened the final paper. This work was supported by NASA's Planetary Geology and Geophysics Program which is gratefully acknowledged.

References

Aydin, A., Ahmadov, R., 2009. Bed-parallel compaction bands in aeolian sandstone: their identification, characterization and implications. Tectonophysics 479, 277–284.
Aydin, A., Borja, R.I., Eichhubl, P., 2006. Geological and mathematical framework for failure modes in granular rock. J. Struct. Geol. 28, 83–98.
Baud, P., Vajdova, V., Wong, T.-f., 2006. Shear-enhanced compaction and strain localization: inelastic deformation and constitutive modeling of four porous sandstones. J. Geophys. Res. 111, B12401. doi:10.1029/2005JB004101.
Bésuelle, P., 2001. Compacting and dilating shear bands in porous rock: theoretical and experimental conditions. J. Geophys. Res. 106, 13,435–13,442.
Bésuelle, P., Rudnicki, J.W., 2004. Localization: shear bands and compaction bands. In: Guéguen, Y., Boutéca, M. (Eds.), Mechanics of Fluid-Saturated Rocks. Elsevier, Amsterdam, pp. 219–321.
Bump, A.P., Davis, G.H., 2003. Late Cretaceous–Early Tertiary Laramide deformation of the northern Colorado Plateau, Utah and Colorado. J. Struct. Geol. 25, 421–440.
Davis, G.H., 1999. Structural geology of the Colorado Plateau region of southern Utah, with special emphasis on deformation bands. Geol. Soc. Am. Spec. Pap. 342.
Davis, G.H., Bump, A.P., 2009. Structural geologic evolution of the Colorado Plateau. In: Kay, S.M., Ramos, V.A., Dickinson, W.R. (Eds.), Backbone of the Americas: Shallow Subduction, Plateau Uplift, and Ridge and Terrane Collision: Geol. Soc. Amer. Mem., 204, pp. 99–124.
Davis, R.O., Selvadurai, A.P.S., 2002. Plasticity and Geomechanics. Cambridge University Press.
Doelling, H.H., Davis, F.D., 1989. The geology of Kane County, Utah. Utah Geol. Mineral Surv. Bull. 124.
Doelling, H.H., Willis, G.C., 2006. Geologic map of the Smoky Mountain 30′×60′ quadrangle, Kane and San Juan Counties, Utah, and Coconino County, Arizona. Utah Geol. Surv. Map 213.
Eichhubl, P., Hooker, J.N., Laubach, S.E., 2010. Pure and shear-enhanced compaction bands in Aztec Sandstone. J. Struct. Geol. 32, 1873–1886.
Fossen, H., Schultz, R.A., Rundhovde, E., Rotevatn, A., Buckley, S.J., 2010. Fault linkage and graben stepovers in Canyonlands (Utah) and the North Sea Viking Graben, with implications for hydrocarbon migration and accumulation. Assoc. Petrol. Geol. Bull. 94, 597–613.
Holcomb, D., Rudnicki, J.W., Issen, K.A., Sternlof, K., 2007. Compaction localization in the Earth and the laboratory: state of the research and research directions. Acta Geotech. 2, 1–15.
Humphreys, E., 2009. Relation of flat subduction to magmatism and deformation in the western United States. In: Kay, S.M., Ramos, V.A., Dickinson, W.R. (Eds.), Backbone of the Americas: Shallow Subduction, Plateau Uplift, and Ridge and Terrane Collision: Geol. Soc. Amer. Mem., 204, pp. 1–13.
Huntoon, P.W., 1993. Influence of inherited Precambrian basement structure on the localization and form of Laramide monoclines, Grand Canyon, Arizona. In: Schmidt, C.J., Chase, R.B., Erslev, E.A. (Eds.), Laramide Basement Deformation in the Rocky Mountain Foreland of the Western United States: Geol. Soc. Amer., Spec. Pap., 280, pp. 243–256.
Issen, K.A., Challa, V., 2008. Influence of the intermediate principal stress on the strain localization mode in porous sandstone. J. Geophys. Res. 113, B02103. doi:10.1029/2005JB004008.
Johnson, K.M., Johnson, A.M., 2002. Mechanical models of trishear-like folds. J. Struct. Geol. 24, 277–287.
Katsman, R., Aharonov, E., 2006. A study of compaction bands originating from cracks, notches, and compacted defects. J. Struct. Geol. 28, 508–518.
Katsman, R., Aharonov, E., Scher, H., 2004. Numerical simulation of compaction bands in high-porosity sedimentary rock. Mech. Mater. 37, 371–390.
King, G.C.P., Cocco, M., 2001. Fault interaction by elastic stress changes: new clues from earthquake sequences. Adv. Geophys. 44, 1–38.
King, G.C.P., Stein, R.S., Lin, J., 1994. Static stress changes and the triggering of earthquakes. Seismol. Soc. Amer. Bull. 84, 935–953.
Lin, J., Stein, R.S., Sevilgen, V., Toda, S., 2010. USGS-WHOI-DPRI Coulomb stress-transfer model for the January 12, 2010, $M_W = 7.0$ Haiti earthquake. U.S. Geol. Surv. Open-File Rep. 2010-1019. 7 p.
Mollema, P.N., Antonellini, M.A., 1996. Compaction bands: a structural analog for anti-mode I cracks in aeolian sandstone. Tectonophysics 267, 209–228.
Okubo, C.H., Schultz, R.A., 2005. Evolution of damage zone geometry and intensity in porous sandstone: insight gained from strain energy density. J. Geol. Soc. London 162, 939–949.
Okubo, C.H., Schultz, R.A., 2004. Mechanical stratigraphy in the western equatorial region of Mars based on thrust fault-related fold topography and implications for near-surface volatile reservoirs. Geol. Soc. Am. Bull. 116, 594–605.
Paterson, M.S., Wong, T.-f., 2005. Experimental Rock Deformation—The Brittle Field, 2nd. ed. Springer, Berlin.
Roznovsky, T.A., Aydin, A., 2001. Concentration of shearing deformation related to changes in strike of monoclinal fold axes: the Waterpocket monocline, Utah. J. Struct. Geol. 23, 1567–1579.
Savage, H.M., Cooke, M.L., 2004. The effect of non-parallel thrust fault interaction on fold patterns. J. Struct. Geol. 26, 905–917.
Schultz, R.A., 2000. Localization of bedding plane slip and backthrust faults above blind thrust faults: keys to wrinkle ridge structure. J. Geophys. Res. 105, 12,035–12,052.
Schultz, R.A., 2003. Seismotectonics of the Amenthes Rupes thrust fault population. Mars. Geophys. Res. Lett. 30, 1303. doi:10.1029/2002GL016475.
Schultz, R.A., 2009. Scaling and paleodepth of compaction bands, Nevada and Utah. J. Geophys. Res. 114, B03407. doi:10.1029/2008JB005876.
Schultz, R.A., Fossen, H., 2008. Terminology for structural discontinuities. Amer. Assoc. Petrol. Geol. Bull. 92, 853–867.
Schultz, R.A., Lin, J., 2001. Three-dimensional normal faulting models of Valles Marineris, Mars, and geodynamic implications. J. Geophys. Res. 106, 16,549–16,566.
Schultz, R.A., Watters, T.R., 2001. Forward mechanical modeling of the Amenthes Rupes thrust fault on Mars. Geophys. Res. Lett. 28, 4659–4662.
Schultz, R.A., Okubo, C.H., Fossen, H., 2010. Porosity and grain size controls on compaction band formation in Jurassic Navajo Sandstone. Geophys. Res. Lett. 37, L22306 2010GL044909.
Shamir, G., Eyal, Y., 1995. Elastic modeling of fault-driven monoclinal fold patterns. Tectonophysics 245, 13–24.
Solum, J.G., Brandenburg, J.P., Kostenko, O.V., Wilkins, S.J., Schultz, R.A., 2010. Characterization of deformation bands associated with normal and reverse stress states in the Navajo Sandstone, Utah. Amer. Assoc. Petrol. Geol. Bull. 94, 1453–1475.
Stanchits, S., Fortin, J., Gueguen, Y., Dresen, G., 2009. Initiation and propagation of compaction bands in dry and wet Bentheim Sandstone. Pure Appl. Geophys. 166, 843–868.
Stein, R.S., 1999. The role of stress transfer in earthquake occurrence. Nature 402, 605–609.
Stein, R.S., King, G.C.P., Lin, J., 1992. Change in failure stress on the southern San Andreas fault system caused by the 1992 magnitude = 7.4 Landers earthquake. Science 258, 1328–1332.
Sternlof, K.R., Rudnicki, J.W., Pollard, D.D., 2005. Anticrack inclusion model for compaction bands in sandstone. J. Geophys. Res. 110, B11403. doi:10.1029/2005JB003764.
Taboada, A., Bousquet, J.C., Philip, H., 1993. Coseismic elastic models of folds above blind thrust faults in the Betic Cordilleras (Spain) and evaluation of seismic hazard. Tectonophysics 220, 223–241.
Tembe, S., Baud, P., Wong, T.-f., 2008. Stress conditions for the propagation of discrete compaction bands in porous sandstone. J. Geophys. Res. 113, B09409. doi:10.1029/2007JB005439.
Tindall, S.E., 2000. The Cockscomb segment of the East Kaibab monocline: taking the structural plunge. In: Sprinkel, D.A., Chidsey Jr., T.C., Anderson, P.B. (Eds.), Geology of Utah's Parks and Monuments: Utah Geol. Assoc., Publ., 28, pp. 1–15.
Tindall, S.E., Davis, G.H., 1999. Monocline development by oblique-slip fault-propagation folding: the East Kaibab monocline, Colorado Plateau, Utah. J. Struct. Geol. 21, 1303–1320.
Toda, S., Stein, R.S., Reasenberg, R.A., Dieterich, J.H., Yoshida, A., 1998. Stress transferred by the 1995 Mw = 6.9 Kobe, Japan, shock: effect on aftershocks and future earthquake probabilities. J. Geophys. Res. 103, 24,543–24,565.
Toda, S., Stein, R.S., Lin, J., Sevilgen, V., 2007. Coulomb 3, Graphic-rich stress change and deformation software for earthquake, tectonic, and volcano research and teaching. Mac/PC/Linux application, 60-p. user guide (http://www.coulombstress.org/).
Vajdova, V., Wong, T.-f., 2003. Incremental propagation of discrete compaction bands: acoustic emission and microstructural observations on circumferentially notched samples of Bentheim Sandstone. Geophys. Res. Lett. 30, 1775. doi:10.1029/2003/GL017750.